

Perspective of fracture mechanics inspired by gap test with crack-parallel compression

Hoang Nguyen^a, Madura Pathirage^a, Masoud Rezaei^b, Mohsen Issa^b, Gianluca Cusatis^a, and Zdeněk P. Bazant^{a,1}

^aDepartment of Civil and Environmental Engineering, Northwestern University, Evanston, Illinois; ^bDepartment of Civil and Materials Engineering, University of Illinois at Chicago

This manuscript was compiled on June 1, 2020

1 **The line-crack models, including linear elastic fracture mechanics**
2 **(LEFM), cohesive crack model (CCM), and extended finite element**
3 **method (XFEM), rest on the century-old hypothesis of constancy of**
4 **materials' fracture energy. However, a new type of fracture test pre-**
5 **sented here, named the *gap test*, reveals that, in concrete and prob-**
6 **ably all quasibrittle materials, including coarse-grained ceramics,**
7 **rocks, stiff foams, fiber composites, wood and sea ice, the effective**
8 **mode I fracture energy depends strongly on the crack-parallel normal**
9 **stress, in-plane or out-of-plane. This stress can double the fracture**
10 **energy or reduce it to zero. Why hasn't this been detected earlier?–**
11 **Because the crack-parallel stress in all standard fracture specimens**
12 **is negligible, and is anyway unaccountable by line-crack models. To**
13 **simulate this phenomenon by finite elements (FE), the fracture pro-**
14 **cess zone must have a finite width, and must be characterized by**
15 **a realistic tensorial softening damage model whose vectorial con-**
16 **stitutive law captures oriented mesoscale frictional slip, microcrack**
17 **opening and splitting with microbuckling. This is best accomplished**
18 **by the FE crack band model which, when coupled with microplane**
19 **model M7, fits the test results satisfactorily. The lattice discrete**
20 **particle model also works. However, the scalar stress-displacement**
21 **softening law of CCM and tensorial models with a single-parameter**
22 **damage law are inadequate. The experiment is proposed as a stan-**
23 **dard. It represents a simple modification of the three-point-bend test**
24 **in which both the bending and crack-parallel compression are stati-**
25 **cally determinate. Finally, a perspective of various far-reaching con-**
26 **sequences and limitations of CCM, LEFM and XFEM is discussed.**

fracture energy | cohesive crack model | Finite element crack band
model | softening damage | quasibrittle materials

1 **T**he linear elastic fracture mechanics (LEFM), origi-
2 nated by Griffith in 1921 (1), and the cohesive crack
3 model (CCM), introduced by Barenblatt in 1959 (2), are
4 line crack models that do not include the crack-parallel
5 strain ϵ_{xx} among the basic thermodynamic variables, and
6 thus cannot take the crack-parallel normal stress σ_{xx} prop-
7 erly into account. This is because a zero width fracture
8 process zone (FPZ) is considered. Thus the crack-parallel
9 normal stress σ_{xx} (Fig 1A) can enter the LEFM or CCM
10 only as a parameter of fracture energy. Then, however,
11 one cannot distinguish different histories of crack-parallel
12 stress, and their effects on the relative displacements of
13 crack faces and on the stress-strain tensors in the FPZ.
14 Therefore, a FPZ of finite width must be modeled, re-
15 flecting its meso-scale physical behavior. The possibilities
16 are a tensorial damage softening constitutive law coupled
17 with crack band model (CBM) (3), the nonlocal models
18 (4), or the lattice discrete particle model (LDPM) (5–7).

19 The softening law must capture the difference between

(a) the total fracture energy, G_F , which represents the
20 area under the traction-separation curve in CCM; and (b)
21 the initial fracture energy, G_f , which is the area under
22 the initial tangent of the traction-separation curve and
23 is the key parameter for predicting the load capacity of
24 concrete specimens and structures (8, 9) (see Fig. 1F).
25 Both CCM and LDPM can capture this difference. Typi-
26 cally, $G_F/G_f \approx 2$ to 6 for concretes. G_f is what governs
27 the maximum loads of most structures, while G_F usually
28 matters only for energy adsorption, e.g., under impact.
29

High crack-parallel stresses are important for all qua-
30 sibritle materials such as concrete, shale, coal and vari-
31 ous rocks, stiff soils, tough or toughened ceramics, bone
32 and many biomaterials, fiber composites, sea ice, printed
33 solids, rigid foams and wood, because these materials
34 exhibit similar mesoscale mechanisms. All brittle ma-
35 terials become quasibrittle on the micro- or nano-meter
36 scales. The importance of considering a finite width of
37 FPZ is supported by futile experience with the cohesive
38 crack modeling of size effect in shear failure of reinforced
39 concrete beams and slabs, which has been a formidable
40 problem for decades. A crack of nearly mode I type, driven
41 by shear force, propagates in a stable manner through
42 about 80% of the cross section depth, and the failure
43 eventually occurs because of crack-parallel compression
44

Significance Statement

Fracture mechanics has long been an essential tool for ensuring safety, efficiency and durability in the mechanical, aerospace, nuclear, naval, petroleum and other industries. Recently, with the adoption of fracture-based size effect law for design code of American Concrete Institute (ACI-318), fracture mechanics has also become the basis of designing concrete structures against quasibrittle failures. The present experimental discovery will improve the fracture predictions for concrete, rock (including shale), fiber composites, tough ceramics, sea ice, wood and other quasibrittle materials.

Z.B. proposed general approach; H.N. and Z.B. designed research and G.C. and M.I. advised on it; H.N. and M.P. produced test specimens; H.N., M.P., M.R. and M.I. performed experiments; H.N., M.P. and M.R. analyzed test results; all discussed the results; H.N. and Z.B. wrote the paper; G.C. improved it.

¹ Address correspondence to: z-bazant@northwestern.edu

at the crack front (Fig. 2C,D). Another example is the gross overestimation of the forces exerted by sea ice on the legs of oil platforms. Neither LEFM nor CCM could ever fit the data but the CBM (with M7) (8, 10–13) and the LDPM (14, 15) could. This experience is what partly inspired this study.

The micro-mechanism of compression damage and fracture in these materials consists of lateral expansion due to splitting and slip along inclined microcracks or along weak interfaces between inhomogeneities. Metals, on the micrometer scale, exhibit progressive strain softening (due to void growth or grain boundary mismatch (16), or to hydrogen embrittlement (17)), and so σ_{xx} must have an effect at that scale, too. Similarly, such stresses play a non-negligible role in hydraulic fracturing of shale at 3 km depth as they are nearly equal to the uniaxial compression strength, σ_c . High σ_{xx} also arises in composite laminates in aircraft and automobile crush cans, sea ice floes pushing against oil platform, pavement cracks, etc.

Relevant Previous Studies. The effect of crack-parallel stresses in quasibrittle materials has been widely ignored. The reason obviously is that, for line-crack models (LEFM, CCM), a line crack cut along x -direction in a uniform field of σ_{xx} causes, of course, no stress change. This might be why all the standard notched fracture test specimens—three-point-bend (3PB), single-edge-notched tension (SENT), circumferentially notched tension (CNT), diametral compression (DC), compact tension (CT), double cantilever, edge-notched eccentric compression, etc.—have near-zero σ_{xx} . The wedge-splitting specimen might seem to be an exception, but the $|\sigma_{xx}|$ is insignificant compared with the uniaxial compression strength, f_c , and is non-negligible only at some distance from the FPZ.

Another reason for experiments with negligible σ_{xx} might have been to shun the complexity of applying additional loads, which leads to ambiguity. In structural engineering labs, tests with multiple loads are, of course, commonplace, but they require the use of multiple hydraulic jacks, which introduce undesirable self-weight loads and lead to a statically indeterminate support system in which stress evaluation requires a damage constitutive law which many be well understood.

Hydraulic jacks causing crack-parallel compression were used in 1995 by Tschegg et al. (18) in an elaborate modification of the wedge-splitting test. The results confirmed the hint from the 1987 microplane model that crack-parallel compression should matter. However, the evaluation was aimed at G_F rather than G_f , and thus was compromised by unknown shape, at that time, of the complete softening law (as in Fig. 1F), and suffered from the complexity of the stress field due to the weight of heavy clamping frames, and to friction under the jacks. Bigger problems were the lack of tests at different sizes, without which the work-of-fracture method is now known to give ambiguous results (19), due to the FPZ size variation

near notch tip and near opposite boundary.

The effect of σ_{xx} , called the T-stress, was also considered in fracture of plastic metals (20–23). Triaxiality of stress state in a tip-surrounding annulus, with extra parameter Q as the relative difference between stress fields when T is or is not zero, led to a monotonic increase of the critical J-integral value based on the Hutchinson-Rice-Rosengren (HRR) (24, 25) field. These results, however, are not transplantable to quasibrittle materials, in which the physics is different (Fig. 2E) and the σ_{xx} effect can be non-monotonic. Moreover, the impact of biaxial in-and-out-of-plane stresses seems not to have been studied for metals. The T-stress effect was also analyzed in (26), but for a different purpose—curved deflection of the LEFM crack path.

In numerical analysis, the simplest and the most widely used method for quasibrittle fracture of concrete and geomaterials is the crack band model (CBM) (3). It requires a realistic tensorial constitutive law for softening damage (27, 28), so as to capture implicitly the mechanisms in Fig. 2E. An alternative is an explicit mesoscale particle model, e.g. (6, 7). The microplane model for concrete, particularly its latest version M7 (CBM-M7) (27, 28) employed here, has been shown to reproduce the dilatant slip and splitting closely. However, the cohesive crack model with a unique traction-separation law for a line crack, the LEFM used in XFEM (29), and the tensorial damage band models governed by a single parameter (30–32), cannot capture the σ_{xx} effect.

Fracture test with crack-parallel compression. To demonstrate and measure the σ_{xx} effect, we develop a surprisingly simple test of notched beams, named the gap test, with four crucial features:

- (i) plastic support pads with near-perfect plastic yielding introduce, at first, notch-parallel compression σ_{xx} ;
- (ii) rigid end supports are installed with gaps and engage only after constant σ_{xx} begins to act, which
- (iii) delivers a support system that switches from one statically determinate configuration to another, thus allowing unambiguous interpretation; and
- (iv) the test is at the same time suitable for the size effect method needed for evaluating the fracture energy G_f and characteristic FPZ size c_f unambiguously.

In this new experiment, depicted in Fig. 1A (as developed at Northwestern University), a notched three-point-bend concrete beam is placed on two kinds of sequentially engaged statically determinate supports: 1) two symmetric pairs of initially contacting polypropylene pads, one pair immediately adjacent to the sides of the notch, and 2) a pair of stiff cylindrical supports installed with initial small gaps at beam ends.

The pads initially deform elastically and subsequently exhibit a long, almost horizontal, yield plateau, shown in Fig. 1B. The magnitude of the maximum yield force, for a given pad area in contact with the specimen, can be

controlled by piercing the pad with holes, which allows applying different levels of stress parallel to the notch. The center-span load is applied through a pair of steel plates located symmetrically to the plastic pads.

Until the support gaps at the ends close, the only loading is by two compression forces along the notch plane, with only negligible bending due to the self-weight. The pair of steel plates at the top is mildly restrained against rotation, to ensure stability. Shortly after the pads begin to yield, the stiff end supports engage in contact and produce a bending moment which increases until the maximum load is reached, while, thanks to plastic yielding of the pads, the crack-parallel compression force remains constant. Thus the bending action, which is what opens the crack, is statically determinate.

The compressive stress in the FPZ, σ_{xx} , which is what matters to the material property, is proportional to, but only slightly smaller than, the compressive stress under the pads, σ_{pad} . The reduction ratio, $r_c = \sigma_{xx}/\sigma_{pad}$, obtained by crack band FE analysis, is about 0.96, although nonlinear analysis would give a slight (and virtually negligible) variation of r_c with P and structure size. To prevent notch mouth corners from shearing off under the pad force, short and thin laminate sheets are glued at bottom adjacent to the notch. Their effect on the stress intensity factor is negligible. The crack-tip opening displacement δ_{CTOD} is measured by an extensometer (Fig. 1A). After reaching P_{max} , the curve of load P versus load-point displacement drops to the yield load value (Fig. 1D) and the beam then fractures completely.

Since the plasticized polymer in the pads is incompressible, it gets squeezed laterally from the pads. The tangential stiffness of the rectangular pads of width $l \ll$ length L can be shown to be $H = L\mu(l/h)^3$ where h = thickness of the plasticized polymer layer, l = its length (in 2D), and μ = tangential shear modulus of the plasticized polymer (with no holes), which is very small but inevitably nonzero (or else the squeezed polymer would flow out like a fluid). H needs to be also very small, and so l/h should be minimized in pad design.

What made the G_f measurement possible was to test specimens of various sizes and apply the size effect method (33), which is the most robust approach to measure the initial fracture energy G_f (and c_f). It has been adopted as an international standard recommendation (34) and endorsed by ACI-446 (35). It is based on the size effect law for quasibrittle fracture (10, 33, 36, 37). It has become the most widely used method for testing G_f of concrete and geomaterials. One advantage is that it necessitates measuring only P_{max} (no postpeak), though for at least three sufficiently different specimen sizes (8, 33, 38). As another advantage, the identification of G_f along with the characteristic FPZ size c_f is reducible to linear regression. Importantly, the derivation of this method (8, 33) is not affected by the crack-parallel stress, neither in-plane σ_{xx} nor out-of-plane σ_{zz} .

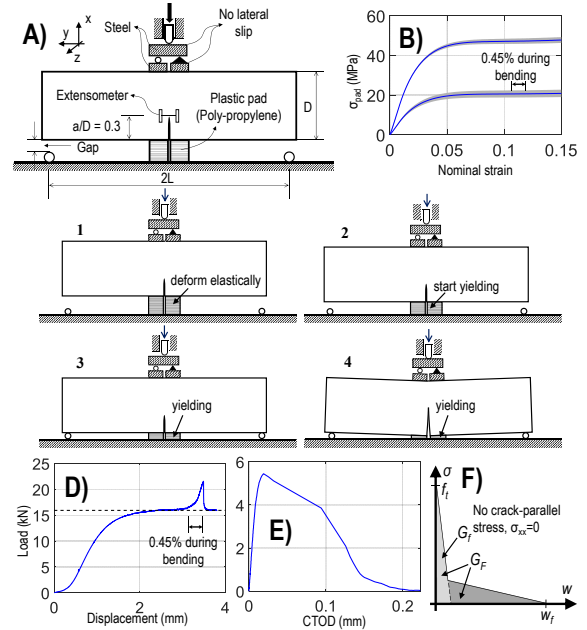


Fig. 1. (A) Experimental setup of the gap test (with coordinates x, y, z); (B) Stress-strain behavior of plastic pad corresponding to two values of tested σ_{xx} ; (C) Experimental procedure; (D) Typical load-machine displacement behavior; (E) Extracted load-CTOD; (F) Traction-separation curve without crack-parallel stress.

The experiments used normal concrete with mean cylindrical compression strength $f_c = 40.5$ MPa, maximum aggregate size 18 mm, span-to-depth ratio $2L/D = 3.75$, and notch depth ratio $a/D = 0.3$. Beams of three depths $D = 101.6$ mm (4 in), 203.2 mm (8 in) and 406.4 mm (16 in), were scaled geometrically. The specimen thickness was 101.6 mm for all sizes. A typical measured curve of load P vs. load-point displacement u and the curve of P versus δ_{CTOD} is shown for $D = 101.6$ mm in Fig. 1D,E.

The three data points (empty circles) in Fig. 2A, based on regression of data from $3 \times 9 = 27$ gap tests, are the evaluated effective values of fracture energy G_f as a function of three levels of compression stress σ_{pad} applied at the yielding pads. Obviously, G_f is not constant but strongly depends on σ_{pad} . This suffices to raise doubts about the applicability of both the LFM and the cohesive crack model, both of which require constancy of G_f . To get the effective G_f as a material property, the data are scaled by r_c to the σ_{xx} values at notch tip—the solid circle points in Fig. 2a.

Alternatively, according to the classical work-of-fracture method (39–41), one could estimate the total fracture energy, G_F , via the area between the whole up-and-down curve and the horizontal yield line in Fig. 1A. However, this method requires stabilizing the postpeak softening and is rather ambiguous if the correct shape of the cohesive law, Fig. 1F, is not known *a priori* (19). To avoid ambiguity of G_F , the work-of-fracture test must be conducted at several sufficiently different specimen sizes (19). Hence, to measure how G_F depends σ_{xx} , the present test would have to be extended into the whole postpeak for all the sizes D .

Fitting and evaluation of test results using microplane model M7.

The simplest and most widely used FE method to suppress spurious mesh sensitivity caused by localization instability of strain-softening damage is the crack band model (3, 8, 42). In a quasibrittle material (i.e., a heterogenous material with brittle constituents and inhomogeneities or grains not negligible compared to structure size), the crack, blunted at front by a long and wide FPZ, is modeled by a band of finite elements (FE) of width h representing a material property; $h = G_{f0}/A$ where A is the area under the curve of stress versus relative displacement and $G_{f0} = G_f$ value for $\sigma_{xx} = 0$. The precise h -value is not too important but the same h must be used for different structure sizes D . Alternatively, if the postpeak of the stress-separation curve is scaled so that Ah would give the same G_f , then h can be changed, with some loss in accuracy. Here, h is kept the same for all D .

The microplane model M7 (27, 28) presented here is the latest version of microplane models whose development began at in 1983. In this model, the damage constitutive law is defined in terms of stress and strain vectors acting on mesoscale planes, called the micro-planes, which sample discretely all spatial orientations according to an optimal Gaussian numerical integration formula for a spherical surface. The use of vectors permits a direct physical modeling of oriented cracking, splitting, and frictional slip, which are crucial for describing the complex stress state in the FPZ. For softening damage, the strain vector is projected from the continuum strain tensor, upon which the stress vectors on all the microplanes are used in the variational principle of virtual work to obtain the stress tensor. M7 has been shown to give good predictions in complex fracture problems and is featured in various softwares. Here M7 is implemented as user-defined material into the commercial software ABAQUS. Six-node wedge elements are used.

The FE program with crack band model and M7 was calibrated so as to give the correct values of uniaxial compression strength and G_f at $\sigma_{xx} = 0$, which is the first data point in Fig. 2A. This calibration sufficed for the FE program with M7 to match closely the tensile material tests. The same FE program was then used to predict the G_f for many applied pressures σ_{pad} , which led to the dashed curve in Fig. 2A, plotted in dimensionless coordinate $\xi_{pad} = \sigma_{pad}/\sigma_c$. Note that this curve matches satisfactorily (within inevitable experimental scatter) the empty circles showing the measured G_f .

However, the plot of G_f vs. ξ_{pad} does not represent a material property. What does is the plot of G_f vs. $\xi = \sigma_{xx}/\sigma_c = r_c \sigma_{pad}/\sigma_{xx}$, corresponding to σ_{xx} values at notch tip. The measured data for G_f are shifted by the same ratio r_c and are shown by the solid circle points. For comparison, ratio r_c calculated by a linearly elastic FE program with a stress-free crack band is $r_{c,el} = 0.942$ for the medium size specimens, 0.981 for the smallest,

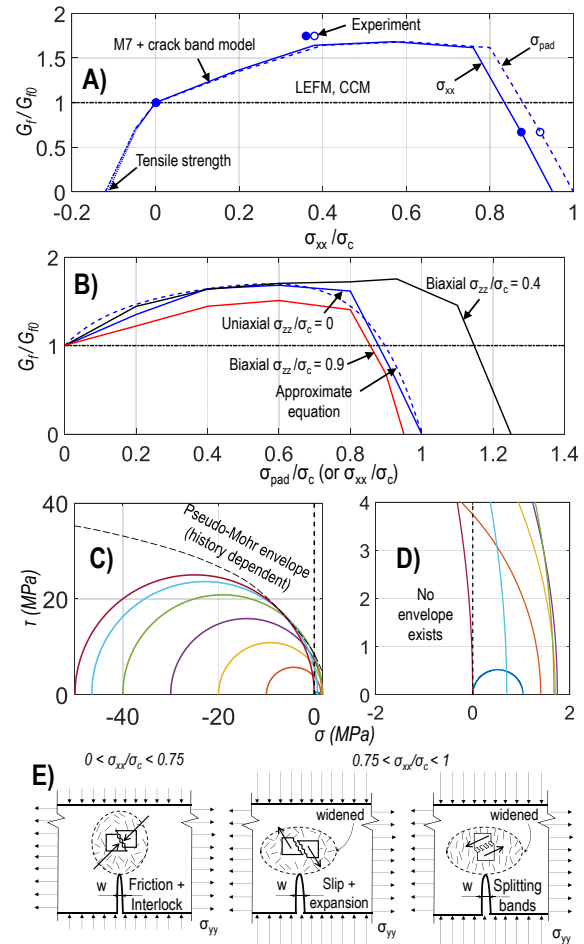


Fig. 2. (A) G_f as a function of σ_{pad} (dashed curve) and of σ_{xx} (solid curve); (B) G_f as a function of σ_{xx} subject to different values of anti-plane stress σ_{zz} ($a = 1.038$, $b = 0.245$, $c = 7.441$ in Eq. 1); (C) Mohr circles corresponding to the M7 results in (A), with σ_{yy} = nominal strength at peak load; (D) A zoom into the region of small σ_{xx} ; and (E) Proposed mechanisms for increase and decrease of G_f .

and 0.925 for the largest; 0.942 is so close 0.962 that $r_{c,el}$ should suffice in practice.

The agreement of the predicted curve with the three data points in Fig. 2A is satisfactory. This observation lends enhanced credence to the new test.

Intuitive explanation of G_f variation by a microstructural mechanism. Can the observed dependence of G_f on crack-parallel stress ratio ξ be plausibly explained physically? It can, by the mechanisms schematized in Fig. 2E (43):

1) To explain the initial rising part of the curve in Fig. 2A, note that a major part of the Mode I fracture energy of concrete is dissipated by frictional slip on microcracks inclined with respect to the directions of macrocrack propagation (44) and by grain interlock enhanced by surface roughness, rather than by opening of tensile microcracks. A pressure on the inclined microcrack as a projection of crack-parallel stress will obviously increase the resistance to slip. This feature explains why, in concrete, the curve

318 of effective G_f versus ξ is initially rising.

319 2) To explain the second, descending, part of the curve
320 in Fig. 2A, note that a higher crack-parallel compression
321 overcomes friction and causes the inclined microcrack to
322 slip, which in turn causes lateral expansion with axial
323 splitting cracks (Fig. 2E). Another possible mechanism is
324 the formation of inclined bands of axial splitting cracks
325 (43), which also leads to slip with lateral expansions (Fig.
326 2E) of width s . Both must cause the FPZ to widen.

327 Can Mohr failure envelope be used to predict incipient
328 failure? The Mohr circles for the subsequent stress states
329 in FPZ are plotted in Fig. 2C,D (σ = hydrostatic stress,
330 τ = maximum shear stress). The first slip mechanism,
331 frictional resistance with no damage, seems to follow a
332 curved Mohr failure envelope with strength expanding
333 at moderate increase of hydrostatic pressure (Fig. 2C).
334 However, when the second mechanism with expansive
335 damage takes over, the Mohr envelope concept breaks
336 down. This is blatantly demonstrated by zooming, in
337 Fig. 2D, on the critical region of small σ and τ . Obvi-
338 ously, no envelope exists. This is not surprising since the
339 plasticity-type failure criteria based on tensor invariants
340 are inherently incapable of capturing the concentration of
341 slip into planes of distinct orientations, which represent
342 the reality.

343 Since the first mechanism is not typical of fiber com-
344 posites, it is suspected that, unlike Fig. 2A,B, their
345 $G_f(\xi)$ -curve would normally be descending monotonically.
346 This would mean that crack-parallel compression is more
347 dangerous than in concrete.

348 Proposal for a new standard fracture test—Gap Test .

349 It now becomes clear that, for quasibrittle materials, the
350 currently standardized fracture tests provide insufficient
351 information. Since, in reinforced concrete, geomechanics
352 or structural composites, cracks with significant crack-
353 parallel compression or tension often occur in finite ele-
354 ment analysis, societies such as ASTM (American Society
355 for Testing and Materials) or RILEM (International Union
356 of Laboratories and Experts in Construction Materials,
357 Systems and Structures, Paris) should consider introduc-
358 ing a standard test. The present test, called Gap Test, is
359 a good candidate.

360 **Vision of fracture mechanics future.** Although the
361 present experiments demonstrate the importance of crack-
362 parallel stress, they are too limited to justify immediate
363 sweeping changes in fracture mechanics practice. Nev-
364 ertheless, in the light of these experiments, it is already
365 obvious that an extensive program of experiments, theo-
366 retical modeling and numerical simulations is called for.
367 Such a program will, of course, require time, significant
368 funding and teams of investigators.

369 So, at this centennial anniversary of Griffith's founding
370 of fracture mechanics (1921), we content ourselves merely
371 with offering a vision of the future.

372 1) It will be necessary to determine all the consequences
373 of crack-parallel compression or tension, in-plane, anti-
374 plane and combined, for the apparent fracture energy in
375 Mode I, and doubtless also modes II and III, and mixed
376 mode—for concretes of diverse types, shale and various
377 other rocks, fiber composites, toughened ceramics, rigid
378 foams, bone, printed solids, sea ice and many other qua-
379 sibrittle materials. Anisotropic materials such as shale
380 or fiber composites will surely show more diversity. Be-
381 cause of the well known weakness in compression of fiber
382 composites, especially the unidirectional ones, and the
383 absence of friction and interlocking, a strong monotonic
384 decrease of effective G_f with crack-parallel compression
385 is expected. The histories of σ_{xx} and σ_{zz} (and probably
386 also in-plane shear stress) will doubtless make a difference,
387 too.

388 2) Major implications can be expected for the hydraulic
389 fracturing of shale, typically conducted at 3 km depth,
390 at which the crack-parallel compression along a vertical
391 crack, due to tectonic stress and overburden, is near the
392 uniaxial strength limit.

393 3) The fracture energy of geological faults causing
394 earthquakes is another tantalizing problem. Very narrow
395 though the fault slip zone is, the FPZ at the front of
396 propagating fault slip might nevertheless be wide enough
397 for the huge tectonic stress parallel to fault to have an
398 effect.

399 4) In view of the mechanism sketched in Fig. 2E, it is
400 expected that, in coarse ceramics, concrete and other qua-
401 sibrittle materials, the crack-parallel compression would
402 accelerate cyclic and static fatigue crack propagation, in-
403 creasing the prefactor of Paris law and Charles-Evans law,
404 and perhaps altering the exponent. The size dependence
405 of these laws (8, 10, 45, 46), particularly the transition
406 size D_0 , might also get modified.

407 5) Fiber reinforcement of concrete tends to mitigate
408 the compression splitting, which is explained by inhibition
409 of the microscale splitting as in Fig. 2E. Fibers are thus
410 expected to prolong the initial rise of the G_f curves in
411 Fig. 2A and to postpone their final descent.

412 6) While the crack-parallel stress has a very different,
413 and already known, effect in plastic-hardening metals, the
414 micrometer scale might be an exception (47) because qua-
415 sibrittle behavior such as gradual postpeak softening with
416 size effect has been observed on thin metallic films. This
417 could matter for micro-electromechanical system (MEMS)
418 substrates and may be worth investigation.

419 7) As it now appears, neither the cohesive crack model,
420 nor the LEFM based models, should be used in general
421 purpose FE softwares for quasibrittle structures. This
422 includes XFEM (29) based on LEFM, and also damage
423 band models based on a one-parameter tensorial damage
424 law (30, 31, 48) which cannot fit the triaxial material tests
425 of various types (27) obtained on specimens of roughly
426 the same size as the FPZ (the so-called "peridynamics"
427 needs no comment (49)). These models are usable only if

it is known a priori that the crack-parallel normal stresses, both in-plane and out-of-plane, are negligible. To capture the effects of these stresses, fracture must be modeled as a band with a realistic tensorial softening damage model, preferably based on vectorial constitutive stress-strain relations that can capture orientation effects, as in microplane or meso-mechanical models such as LDPM.

8) The need for tensorial characterizations of FPZ was suggested in a recent approach (50, e.g.) in which a band with softening constitutive damage law is shrunk into a line, so as to enrich the stress-displacement relation of a cohesive line crack by ϵ_{xx} as an additional parameter. A step in the right direction though this was, the formulation was not shown capable of describing the crack-parallel stress effects and reproducing the effects of triaxial stress history and of nonproportional evolution of stress and strain tensor components in the FPZ. Also, after shrinking the damage band of finite width into a line crack, the minimum possible spacing of parallel cracks does not get enforced.

9) The importance of considering a tensorial FPZ of finite width, as in crack band model, or material heterogeneity as in LDPM, is blatantly demonstrated by: a) the futile experience with the LFM and CCM of size effect in shear failure of RC beams and slabs, or b) gross overestimation of the measured force exerted on the legs of oil platforms by a moving ice plate.

10) The Mohr failure envelope has been widely used to assess incipient fracture of shale, and slip in geophysics. However, due to high σ_{xx} , this is unrealistic.

11) The curve in Fig. 2A,B can be closely approximated by

$$G_f/G_{f0} = 1 + a/(1 + b/\xi) - (1 + a + b)/(1 + b)\xi^c \quad [1]$$

where f_c = compression strength. Constants a, b, c are different for different materials, structure sizes, load histories, σ_{zz}/σ_{xx} ratios, etc. Having such formulas for various situations, the existing softwares for cohesive cracks, LFM, XFEM or phase-field model could be adapted to variable fracture energy, as a crude approximation. But there seems no good general way to avoid crack band or meso-scale simulations.

Afterthought: Many hot research subjects become closed in a few decades. But, like turbulence, fracture mechanics is different. This formidable subject has been researched for a century, and probably will for another century.

Acknowledgement: Partial preliminary funding under NSF Grant CMMI-1439960 to Northwestern. Valuable comments by Jialing Le and Marco Salviato.

Conflict of Interest: None.

Data availability: The data from the experiments and simulations can be found at the author's Github repository: github.com/htn403/PNAS_MS-2020-05646.

1. Griffith A (1921) The phenomena of rupture and flow in solid, Philosophical Translation in *Royal Soc of London, Series A*. Vol. 221. 481
2. Barenblatt G (1959) Equilibrium cracks formed on a brittle fracture. *Dokl. Ak. N.* 127:47–50. 482
3. Bažant ZP, Oh BH (1983) Crack band theory for fracture of concrete. *Mat. Constr.* 16:155–177. 483
4. Bažant ZP, Jirásek M (2002) Nonlocal integral formulations of plasticity and damage: survey of progress. *J. Eng. Mech.* 128:1119–1149. 484
5. Cusatis G, Bažant ZP, Cedolin L (2003) Confinement-shear lattice model for concrete damage in tension and compression: I. theory. *J. Eng. Mech.* 129:1439–1448. 485
6. Cusatis G, Pelessone D, Mencarelli A (2011) Lattice discrete particle model (LDPM) for failure behavior of concrete. i: Theory. *Cem. Concr. Compos.* 33:881–890. 486
7. Cusatis G, Mencarelli A, Pelessone D, Baylot J (2011) Lattice discrete particle model (LDPM) for failure behavior of concrete. ii: Calibration and validation. *Cem. Concr. Compos.* 33:891–905. 487
8. Bažant ZP, Planas J (1998) *Fracture and Size Effect in Concrete and Other Quasibrittle Materials*. CRC Press, Boca Raton, FL. 488
9. Cusatis G, Schaufert EA (2009) Cohesive crack analysis of size effect. *Eng. Fract. Mech.* 76:2163–2173. 489
10. Bažant ZP (2002) *Scaling of structural strength*. CRC Press, Boca Raton, FL. 490
11. Bažant ZP, Yu Q (2005) Designing against size effect on shear strength of reinforced concrete beams without stirrups: II. verification and calibration. *J. Struct. Eng.* 131:1886–1897. 491
12. Yu Q, et al. (2016) Comparison of main models for size effect on shear strength of reinforced and prestressed concrete beams. *Struct. Concr.* 17:778–789. 492
13. Dönmez A, Bažant ZP (2017) Size effect on punching strength of reinforced concrete slabs with and without shear reinforcement. *ACI Struct. J.* 114:875. 493
14. Alnaggar M, Pelessone D, Cusatis G (2019) Lattice discrete particle modeling of reinforced concrete flexural behavior. *J. Struct. Eng.* 145:04018231. 494
15. Lale E, Rezakhani R, Alnaggar M, Cusatis G (2018) Homogenization coarse graining (hcg) of the lattice discrete particle model (LDPM) for the analysis of reinforced concrete structures. *Eng. Fract. Mech.* 197:259–277. 495
16. Bažant ZP, Guo Z, Espinosa HD, Zhu Y, Peng B (2005) Epitaxially influenced boundary layer model for size effect in thin metallic films. *J. Appl. Phys.* 97:073506–1–13. 496
17. Deng Y, Barnoush A (2018) Hydrogen embrittlement revealed via novel in situ fracture experiments using notched micro-cantilever specimens. *Acta Mater.* 142:236–247. 497
18. Tschegg E, Elser M, Stanzl-Tschegg S (1995) Biaxial fracture tests on concrete—development and experience. *Cem. Concr. Compos.* 17:57–75. 498
19. Hoover CG, Bažant ZP (2014) Cohesive crack, size effect, crack band and work-of-fracture models compared to comprehensive concrete fracture tests. *Int. J. Fract.* 187:133–143. 499
20. O'Dowd N, Shih C (1991) Family of crack-tip fields characterized by a triaxiality parameter—I. structure of fields. *J. Mech. Phys. Solids.* 39:989–1015. 500
21. O'Dowd N, Shih C (1992) Family of crack-tip fields characterized by a triaxiality parameter—II. fracture applications. *J. Mech. Phys. Solids.* 40:939–963. 501
22. Betegón C, Hancock J (1991) Two-parameter characterization of elastic-plastic crack-tip fields. *J. Appl. Mech.* 58:104–110. 502
23. Tvergaard V, Hutchinson JW (1992) The relation between crack growth resistance and fracture process parameters in elastic-plastic solids. *J. Mech. Phys. Solids.* 40(6):1377–1397. 503
24. Hutchinson J (1968) Singular behaviour at the end of a tensile crack in a hardening material. *J. Mech. Phys. Solids.* 16:13–31. 504
25. Rice J, Rosengren GF (1968) Plane strain deformation near a crack tip in a power-law hardening material. *J. Mech. Phys. Solids.* 16:1–12. 505
26. Cotterell B, Rice J (1980) Slightly curved or kinked cracks. *Int. J. Fract.* 16:155–169. 506
27. Caner FC, Bažant ZP (2013) Microplane model M7 for plain concrete. i: Formulation. *J. Eng. Mech.* 139:1714–1723. 507
28. Caner FC, Bažant ZP (2013) Microplane model M7 for plain concrete. ii: Calibration and verification. *J. Eng. Mech.* 139:1724–1735. 508
29. Moës N, Dolbow J, Belytschko T (1999) A finite element method for crack growth without remeshing. *Int. J. Numer. Methods Eng.* 46:131–150. 509
30. Bourdin B, Francfort GA, Marigo JJ (2008) The variational approach to fracture. *J. Elast.* 91:5–148. 510
31. Borden MJ, Verhoosel CV, Scott MA, Hughes TJ, Landis CM (2012) A phase-field description of dynamic brittle fracture. *Comput. Meth. in Appl. Mech. & Engrg.* 217:77–95. 511
32. Vignollet J, May S, De Borst R, Verhoosel CV (2014) Phase-field models for brittle and cohesive fracture. *Meccanica* 49:2587–2601. 512
33. Bažant ZP, Kazemi MT (1990) Size effect in fracture of ceramics and its use to determine fracture energy and effective process zone length. *J. Am. Ceram. Soc.* 73:1841–1853. 513
34. TC89-FMT RR (1990) Size-effect method for determining fracture energy and process zone size of concrete. *Mater. Struct.* 23:461. 514
35. ACI Committee 446 (1992) Fracture mechanics of concrete: Concepts, models and determination of material properties. 91. 515
36. Bažant ZP (1984) Size effect in blunt fracture: concrete, rock, metal. *J. Eng. Mech.* 110:518–535. 516
37. Bažant Z (1997) Scaling of quasibrittle fracture: asymptotic analysis. *Int. J. Fract.* 83:19. 517
38. Bažant ZP, Le JL (2017) *Probabilistic mechanics of quasibrittle structures: strength, lifetime, and size effect*. Cambridge University Press. 518
39. Nakayama J (1965) Direct measurement of fracture energies of brittle heterogeneous materials. *J. Am. Ceram. Soc.* 48:583–587. 519
40. Tattersall HG, Tappin G (1966) The work of fracture and its measurement in metals, ceramics and other materials. *J. Mater. Sci.* 1:296–301. 520
41. Hillerborg A, Modéer M, Petersson PE (1976) Analysis of crack formation and crack growth in concrete by means of fracture mechanics and finite elements. *Cem. Concr. Res.* 6:773–781. 521
42. Červenka J, Bažant ZP, Wierer M (2005) Equivalent localization element for crack band approach to mesh-sensitivity in microplane model. *Int. J. Numer. Meth. in Eng.* 62(5):700–726. 522
43. Bažant ZP, Xiang Y (1997) Size effect in compression fracture: splitting crack band propagation. *J. Eng. Mech.* 123:162–172. 523

- 565 44. Bažant ZP, Schell WF (1993) Fatigue fracture of high-strength concrete and size effect. *ACI*
566 *Mater. J.* 90:472–472.
- 567 45. Bažant ZP, Xu K (1991) Size effect in fatigue fracture of concrete. *ACI Mater. J.* 88:390–399.
- 568 46. Kirane K, Bažant ZP (2015) Microplane damage model for fatigue of quasibrittle materials:
569 Sub-critical crack growth, lifetime and residual strength. *Int. J. Fatigue* 70:93–105.
- 570 47. Espinosa HD, Prorok B, Peng B (2004) Plasticity size effects in free-standing submicron
571 polycrystalline fcc films subjected to pure tension. *J. Mech. Phys. Solids.* 52:667–689.
- 572 48. Bourdin B, Francfort GA, Marigo JJ (2000) Numerical experiments in revisited brittle fracture.
573 *J. Mech. Phys. Solids.* 48:797–826.
- 574 49. Bažant ZP, Luo W, Chau VT, Bessa MA (2016) Wave dispersion and basic concepts of peri-
575 dynamics compared to classical nonlocal damage models. *J. Appl. Mech.* 83.
- 576 50. Remmers JJ, De Borst R, Verhoosel CV, Needleman A (2013) The cohesive band model: a
577 cohesive surface formulation with stress triaxiality. *Int. J. Fract.* 181:177–188.